Chapter 10
Personalized Computational Models of the Heart for Cardiac Resynchronization Therapy

Maxime Sermesant and Reza Razavi

10.1 Introduction

Cardiovascular diseases (CVD) are the major cause of morbidity and mortality in the western world. Within CVD, the increasing prevalence of congestive heart failure (CHF) is mainly caused by the steadily increasing number of heart attack survivors. They suffer an important scar burden on their cardiac function due to the infarction. Moreover, CHF has a terrible prognosis with 50% mortality in the first 3 years after diagnosis. Of all CHF patients, those with an additional dyssynchronous contraction have the worst prognosis. Cardiac resynchronization therapy (CRT) involves placing a pacemaker to improve the synchronicity of cardiac contraction. It has recently been shown to be an effective method of treating patients with dyssynchronous CHF, inducing significant reductions in morbidity and mortality in large clinical trials. However, clinical trials have also demonstrated that up to 30% of patients may be classified as nonresponders. There remains major controversy surrounding patient selection and optimization of this expensive treatment (e.g., lead positioning, pacemaker setting). For instance, recent studies showed that patients with heart failure and narrow QRS intervals do not currently benefit from CRT (RethinQ, [3]) and that no single echocardiographic measure of dyssynchrony may be recommended to improve patient selection (PROSPECT, [10]). Therefore, new approaches are needed in order to provide a better diagnosis and characterization of patients while achieving a better planning and delivery of the therapy.

In parallel, the last decades have seen major progress in medical imaging, cardiac modeling, and computational power that make personalized simulations (i.e., using models with patient-specific parameters) achievable. While the scientific importance and enormous clinical potential of this approach have been acknowledged [12, 23], its translation into clinical applications remains largely to be done. We aim to build

M. Sermesant (✉)
Asclepios Team INRIA, 2004 route des Lucioles, 06 902, Sophia Antipolis, France
e-mail: maxime.sermesant@inria.fr

R.C.P. Kerckhoffs (ed.), *Patient-Specific Modeling of the Cardiovascular System: Technology-Driven Personalized Medicine*, DOI 10.1007/978-1-4419-6691-9_10,

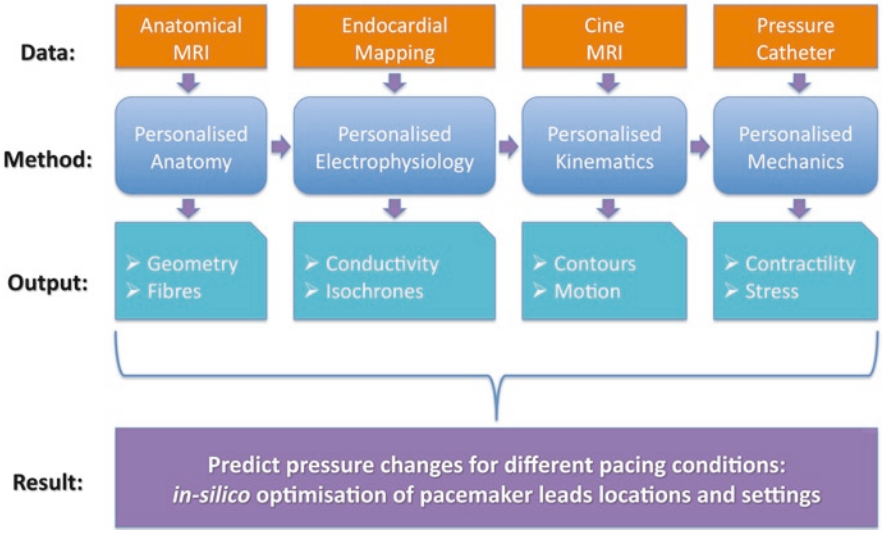

Fig. 10.1 Global scheme of the clinical data used for the personalized models, the generated output maps and parameters, and the resulting predictions [54]

on the major scientific progress that has already been made in cardiac modeling, in order to proceed to the next level and personalize such models to each specific patient using state-of-the-art multimodal imaging. This personalization of models has the potential to have a major impact on clinical practice. Indeed, patient management would be improved by a more accurate diagnosis and characterization, and personalized and predictive therapy planning for that specific patient could be achieved.

In this chapter, we demonstrate a proof of concept on a first case study of how the personalization of an electromechanical model of the heart can predict the changes in cardiac function due to changes in pacing (Fig. 10.1). Such predictions can be used to quantify the improvement in cardiac function that can be expected from CRT and also to optimize the location and delays of the pacemaker leads (stimulation electrodes). In this work we only focus on the acute effects of resynchronization. There is also an important part of the therapy process due to the reverse remodeling of the heart under the new pacing conditions [58], but this is out of the scope of the presented work.

There is a growing body of literature on the functional imaging of the heart, for instance with the measurement of electrical activity, deformation, flows, fiber orientation [15, 28, 31, 32], and on the modeling of the electrical and mechanical activity of the heart [24, 33, 39, 42, 63]. Many of these models are *direct* computational models, designed to reproduce the cardiac activity in a realistic manner, often requiring high computational costs and the manual tuning of a very large set of parameters.

Recently, computational models have been used to simulate CRT on a generic anatomy and compared with animal experiments [26, 27], which provide important insights on the pathophysiology of dyssynchrony. However, in order to translate to the clinics and impact the patient management and the therapy planning, such models

need to be personalized (i.e., with adjusted parameters) to the specificity of each patient, which is still a very challenging task.

The proposed approach involves models whose complexity is directly related to the phenomena observed in clinical data. This is the reason why these models are often simplified compared to the very detailed models available in the literature. The observability of their parameters is crucial in the personalization step. Involving a limited number of parameters can allow their identification from clinical measurements on a specific patient by the resolution of a tractable *inverse* problem (Fig. 10.1).

We illustrate in this chapter the personalization of several components. A preliminary section details the clinical context, the data acquisition, and the data fusion into the same spatio-temporal coordinates. We then present the four sections concerning the personalization of the model anatomy, electrophysiology, kinematics, and mechanics. Finally, we demonstrate this first proof of concept on the prediction of the cardiac function and its agreement to interventional measurements for five different pacing conditions on each of the two clinical cases presented.

10.2 Clinical Context, Data Acquisition, and Fusion

The construction, testing, and personalization of biophysical models rely on the ability to fuse data from an array of sources. For cardiac modeling, the fusion of anatomical, mechanical, and electrical data is of primary importance. This fusion must be both in the spatial and temporal domains. High-quality cardiac anatomical and functional data can be obtained from both computerized tomography and magnetic resonance imaging (MRI). MRI can also be used to obtain functional data such as myocardial wall motion and blood flow. Electrical data can be obtained from catheter-based measurements that are guided using X-ray fluoroscopy.

Spatial fusion of these different data requires an effective image registration strategy. Our solution has focused on the use of the X-ray/MR (XMR) hybrid imaging system that allows the seamless collection of both MRI and X-ray-based data (Fig. 10.2). We have developed a real-time registration solution [48] that allows the spatial integration of MRI-based anatomical and functional data with X-ray-based catheter data, such as intracardial electrical and pressure signals. For the temporal integration, the electrocardiogram (ECG) gives information on the heart rhythm that enables the synchronization of the different datasets.

The first patient of this study is a 60-year-old woman with NYHA class III symptoms. The etiology of heart failure is thought to be dilated cardiomyopathy although cardiac MRI did show two nonviable areas of a moderate size corresponding to the drainage area of the left anterior descending (in the apical and mid-inferoseptal segments) and of the left circumflex coronary artery [mid-inferolateral segment of the left ventricle (LV)], which are consistent with a previous subendocardial infarction. However, there was no flow-limiting disease on coronary angiography. Ejection fraction of the LV was around 30% on maximal tolerated medication. The patient suffers from a left bundle branch block as revealed in the ECG, with in particular a QRS duration of 144 ms (while a normal QRS is less than 100 ms). Echocardiography,

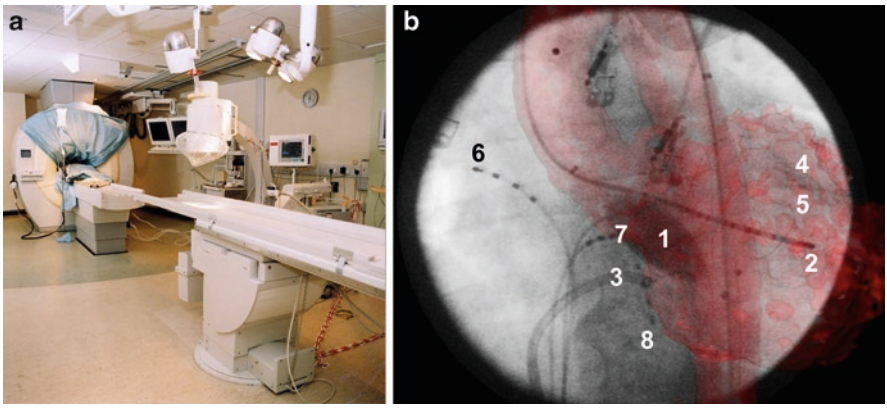

Fig. 10.2 (**a**) XMR suite with the MR scanner and the X-ray C-arm. (**b**) Overlay of MRI-derived left ventricular (LV) surface model onto live X-ray fluoroscopy image. This real-time overlay was used to guide the placement of catheters prior to the start of pacing. The catheters are as follows: (1) St. Jude ESI balloon; (2) LV roving; (3) coronary sinus sheath; (4) coronary venous/epicardial; (5) pressure; (6) high right atrium; (7) His bundle; and (8) right ventricle

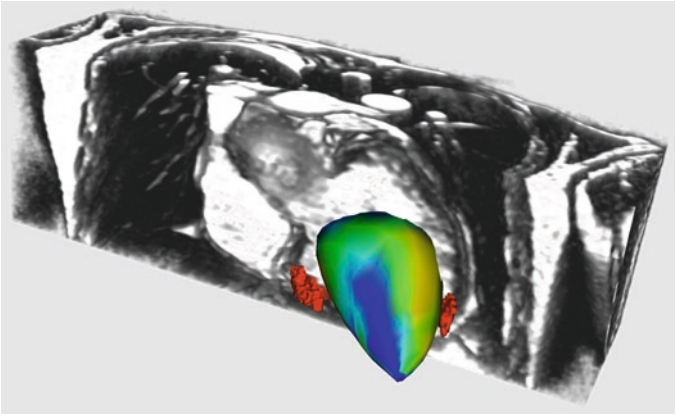

Fig. 10.3 Fusion of late enhancement derived scars (*red surfaces*), anatomical MR (volume rendering) and Ensite isochronal map (colored surface)

including tissue Doppler, confirmed significant mechanical dyssynchrony in keeping with the ECG findings.

The MR examination sequences involve SSFP Cine MR imaging for the estimation of ventricular function and volumes, late enhancement images with gadolinium for scar anatomy, and whole heart 3D navigated free breathing sequences for coronary venous anatomy. The noncontact mapping is performed using the ESI 3000 multielectrode array catheter system (St Jude, Sylmar, CA). This consists of a 64 laser-etched wire braid mounted on an 8 mm balloon. The array records intracavity far-field potentials. The resulting signals are allowing a reconstruction of over 3,000

virtual unipolar electrograms superimposed on a computerized model of the LV, creating both isopotential and isochronal maps. The scar anatomy was manually delineated in late enhancement images. The XMR fusion provides the location of the ESI mapping with respect to the MR-derived information (Fig. 10.3).

10.3 Personalized Anatomy

In this work, the anatomy model we use is limited to the compact biventricular myocardium. As we do not model the valves, we do not simulate the papillary muscles and we only integrate the blood flows in the atria and arteries as preload and afterload boundary conditions. There is an important literature on the segmentation of the heart from medical images, see for instance [14] and references therein. However, to cope with extreme and variable anatomies due to pathologies, we developed a simple yet efficient method, which combines specific image processing tools to extract the biventricular myocardium from Cine-MRI. We segment in the mid-diastolic volume of the cardiac sequence the LV endocardium, the right ventricle (RV) endocardium and the epicardium. To this aim, we developed an interactive tool based on variational implicit functions [62]. This tool allows the user to intuitively model any 3D surface in the 3D scene by placing, moving, or deleting control points inside, on and outside the desired surface [61].

We then extract the surface mesh from the volumetric binary mask and build the volumetric tetrahedral anatomical model from the surface mesh. For personalization of the simulation, each tetrahedron is automatically labeled according to the anatomical region it belongs to (LV, RV, and scar tissue, see Fig. 10.4). The scar label is based on the expert manual delineation on late enhancement MRI. Also, for regional parameter estimation, the mesh was subdivided according to the 17-segment model proposed by the American Heart Association.

The complex cardiac fiber architecture has an important role in the electrical and mechanical functions of the heart. The introduction of the fiber orientation in cardiac electromechanical modeling is essential for simulating properly the cardiac functions.

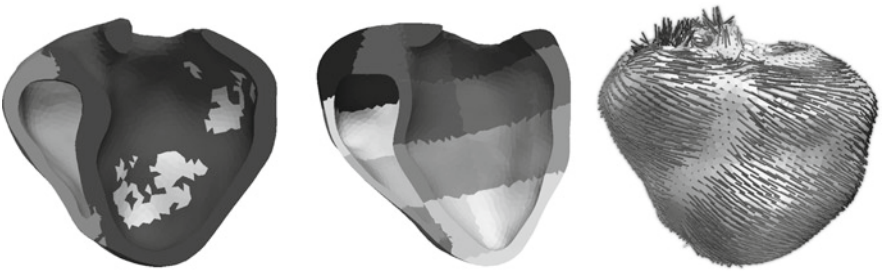

Fig. 10.4 Labeled volumetric mesh. Three main areas are defined. *Left panel*: left ventricle, right ventricle, and scar *(in white)*. *Mid panel*: Additional AHA segments subdivision is also performed for regional personalization. *Right panel*: Fiber orientations assigned to the mesh

The lack of accurate in vivo measurement of these orientations at high resolution [13] yields to using prior knowledge. Synthetic models were built with analytical laws describing general trends of fiber orientations observed in different studies [57]. The complete 3D reconstruction of fiber orientations from histological slices [40] and, more recently, its direct 3D acquisition on ex vivo hearts with diffusion tensor magnetic resonance imaging (DT-MRI) [21] have been used for a more realistic description of the myofiber architecture. However, it still comes from a single subject and thus do not take into account any inter-subject variability. We preferred to use here a statistical atlas of the cardiac fiber architecture [45]. This atlas was computed from a population of ex vivo canine hearts but was showed to be consistent with human hearts [46]. We use this atlas to generate cardiac fiber orientations, by setting the parameters of an analytical model of these fibers according to the angles observed in the atlas (Fig. 10.4, see also Chaps. 7 and 9). The personalized anatomy encompassing a computational mesh of the compact biventricular myocardium and the local fiber orientations is used for the electrophysiology model personalization described in the next section.

10.4 Personalized Electrophysiology

Clinical electrophysiological data currently available only reliably describe the depolarization times, and not the extracellular or transmembrane potentials. So we chose our electrophysiology model accordingly. Modeling the cell electrophysiology (EP) has been an active research area since the seminal work of Hodgkin and Huxley [18]. At the organ level, it involves a cell membrane model embedded into a set of partial differential equations (PDEs) representing a continuum. There are three main categories, in decreasing order of computational complexity.

- Biophysical: Semi-linear reaction-diffusion dynamic PDEs with ionic models (over 50 equations for ions and channels) [2, 30, 41, 43, 59].
- Phenomenological: Semi-linear reaction-diffusion dynamic PDEs with mathematical simplifications of the biophysical models (bidomain, monodomain) [1, 16, 47].
- Eikonal: One static nonlinear PDE for the depolarization time derived from the previous models (Eikonal-Curvature, Eikonal-Diffusion) [11, 25].

Solving the dynamic PDEs is computationally very demanding, due to the space scale of the electrical propagation front being much smaller than the size of the ventricles, and the stability issues of the dynamic aspect. The Eikonal equation is static, and the front can be observed at a larger scale, resulting in much faster computations. An anisotropic multifront fast marching method was developed in order to solve the Eikonal model equations very efficiently [52]. We base our model on the Eikonal diffusion (ED) equation (see [60] for more details on the ED equation and its parameters).

To personalize the electrophysiology model, there are two important adjustments to perform: the onset of the electrical propagation and the local conduction velocity, which corresponds to an apparent conductivity (AC). The idea is to estimate the AC by matching the simulated propagation times of the model to the clinically measured

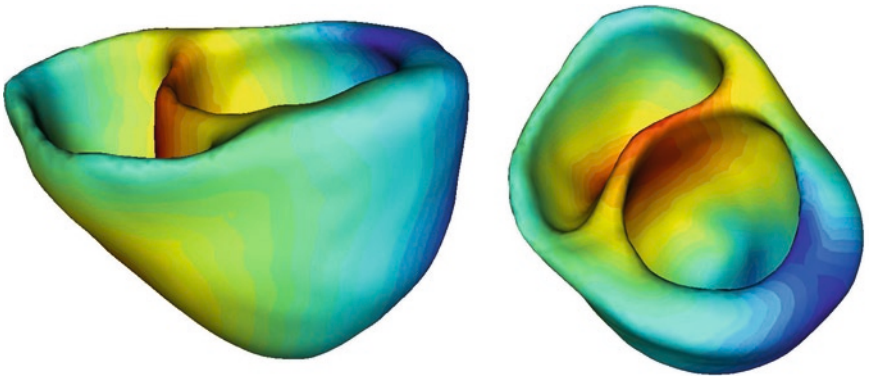

Fig. 10.5 Simulated isochrones on the volumetric mesh, adjusted using the endocardial mapping as reference. Color encodes the depolarization time (*red*: 0 ms, *blue*: 130 ms)

propagation times of the patient. The automatic adjustment method of the AC was designed for surfaces [8, 9, 37].

Such approaches were extended to volumetric models, by using a coupled error criterion both on endocardial depolarization times and QRS duration. When applying this method to the baseline data, we obtain a very good fit to the data with a final mean error that drops to 3.8 ms. The resulting AC map (Fig. 10.5) provides information on some potential Purkinje network (high values) and does seem to correlate with the scars locations (low values).

10.5 Personalized Electromechanical Models

The myocardium constitutive law has to model the active, nonlinear, anisotropic, incompressible, and visco-elastic properties of the cardiac tissue. Numerous ones were proposed in the literature, see, e.g., [6, 19–22, 38, 49, 55] and references therein. The particularity of the models used here is that they were designed to have a complexity compatible with the clinical data used for the personalization. As apparent motion and left ventricular pressure are the main components of the observations, we rely on models with limited parameters representing the passive and active parts of the constitutive law.

We use two different electromechanical models for the muscle contraction, depending on the application. We first introduce a simplified model as a deformable model in order to extract the motion and contours from the dynamic images (Sect. 10.5.1). We then use this information with additional pressure data in order to personalize a more complex model of the myocardium mechanics, which allows to adjust contractility and estimate pressures (Sect. 10.5.2). The cardiac mechanical models that we use here were presented in detail in [51] and [50]. They rely on the following key ingredients.

- An electrically activated constitutive equation based on a multiscale approach accounting for the behavior of myosin molecular motors, as originally presented in [4].
- A 3D continuum mechanics formulation integrating this active behavior (acting along the muscle fibers) with 3D passive visco-elastic components (based on hyper-elastic potentials and viscous pseudo-potentials) using a rheological model of Hill–Maxwell type [17].

To carry out simulations, additional needs are Windkessel models and valve laws to represent the blood flows, and adequate finite element and energy-preserving time discretization strategies.

We present in the two following subsections how a simplified model is used to estimate the cardiac motion, and then how a more complex model is used to simulate the cardiac mechanics.

10.5.1 Personalized Kinematics

In this subsection, we show a deformable model approach to estimate the motion of the heart using Cine-MRI data and an electromechanical model. The model used here is a simplified electromechanical model designed for cardiac image analysis and simulation [51]. We want the complexity of the model to match the relatively sparse measurements. Thus, we use here a simplified electromechanical model derived from a multiscale modeling of the myocardium described in [4]. It is composed of two elements. The first one is a parallel element which is anisotropic linear visco-elastic and which represents the passive properties of the tissue. The second one is an active contractile element controlled by the electrophysiological command. Furthermore, we simulate the four cardiac phases (filling, isovolumetric contraction, ejection, and isovolumetric relaxation) as detailed in [51]. Finally, the arterial pressures were computed using a three-element Windkessel model described in [56].

We estimate the motion of the heart by coupling an electromechanical model and Cine-MRI data, based on the proactive deformable model described in [51]. We have shown in [5] that this method is related to the data assimilation approach described in [35]. Numerous works on the adjustment of a geometrical model of the heart to time series of medical images are based on the concept of deformable models [34, 36, 44]. In this framework, a surface is fitted to the apparent boundaries of the myocardium by minimizing the sum of two energies: a data attachment term and a regularization term. In our case, this regularization term consists in the energy of the dynamical system of the simplified electromechanical model of the heart.

We want to minimize the difference between the simulated motion of the myocardium and the apparent motion in the images. As Cine-MRI only provides the

apparent (radial) motion of the endocardium (we do not have information on the tangential motion), we use the distance from the contours detected in the images to the mesh. To compute it, we seek for each surface vertex the closest boundary voxel (based on criteria on the image gradient) along the normal direction of the mesh. We then apply a force in that direction, proportional to the distance to this boundary voxel.

Figure 10.6 shows the MR images at end-diastole and at end-systole of the cardiac cycle. The superimposed lines represent the endocardium and epicardium surfaces of the estimated mesh. Colors correspond to the intensity of the image forces.

We can observe that despite the limited quality of clinical routine images, the estimation of the myocardium contours is good, especially for the LV. Due to the lack of contrast on the epicardium and the small thickness of the RV, achieving a good dynamic segmentation of the RV is still very challenging. This approach allows estimating a complete motion, including the twisting of the heart, while only using the data where it is reliable, which is in the normal direction for Cine-MRI. This estimated motion is then used to guide the adjustment of a more complex model in order to simulate the pressure variation in the ventricles.

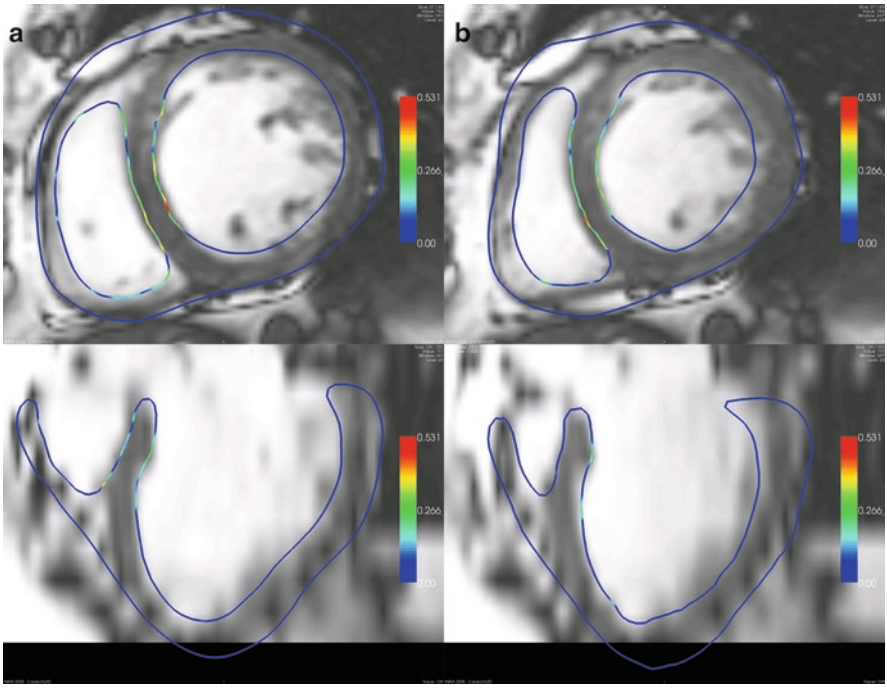

Fig. 10.6 Results of the motion tracking: delineation of the estimated mesh superimposed with Cine-MRI at (**a**) end-diastole and (**b**) end-systole. Color encodes the intensity of the image forces (*blue*: small, *red*: large) [54]

10.5.2 Personalized Mechanics

We now utilize the estimated motion to personalize the mechanical parameters, in a more complex model in order to ensure a realistic simulation of the stress. Most of the components of the mechanical model discussed in this section (detailed in [50]) are quite classically used in heart models. Nevertheless, the emphasis and originality of our approach lies in the careful choice of modeling ingredients that are relevant from a physiological point of view and consistent with essential thermo-mechanical requirements and in their global integration in ways that preserve these requirements at all steps, from the continuous dynamical equations to the discrete versions with which actual simulations are performed.

This active constitutive law was used within a rheological model of Hill–Maxwell type [7]. This rheological model is compatible with large displacements and strains and led to a continuum mechanics description of the cardiac tissue [50]. In the parallel branch of the Hill–Maxwell model we considered a visco-elastic behavior, with a hyper-elastic potential given by the Ciarlet–Geymonat volumic energy [29]. The pressure within the ventricles is then an output of the model simulation.

Adjusting the material parameters is made difficult by the fact that we are concerned with patients whose parameter values differ from nominal ones in pathological regions, e.g., decreased contractility and increased stiffness in infarcted parts. Some valuable information on the spatial distribution of these pathological regions may be obtained from clinical measurements such as late enhancement MRI, but the actual values of the perturbed parameters cannot be directly measured. Therefore, the objective of (automatically) estimating the parameter values – using some appropriate data assimilation procedures – is of utmost clinical interest. Such a complete automated estimation – still a major scientific challenge – is out of the scope of the present chapter, but we demonstrate that a proper calibration of the parameters based on global physiological indicators and using the personalization steps presented above can provide satisfactory predictability in the direct simulation of the cardiac function.

For this simulation where image information is no longer used, boundary conditions are especially important. As can be seen, e.g., in MRI sequences, there is an epicardium area near the apex on the inferior wall with small displacements, probably in relation with the attachment of the pericardium to the diaphragm. We modeled this physiological feature by prescribing some stiff visco-elastic support as boundary conditions in this area. Furthermore, we used similar visco-elastic support conditions on the base to model the truncated anatomy. The corresponding visco-elastic coefficients also require proper calibration with respect to the kinematics observed in image sequences.

The other anatomical and electrophysiological parameters have been set as in the previous sections. The mechanical parameters have been calibrated using the pressure–volume medical indicators, and also the MRI sequence as explained above for the boundary conditions. In order to take into account the infarct, the

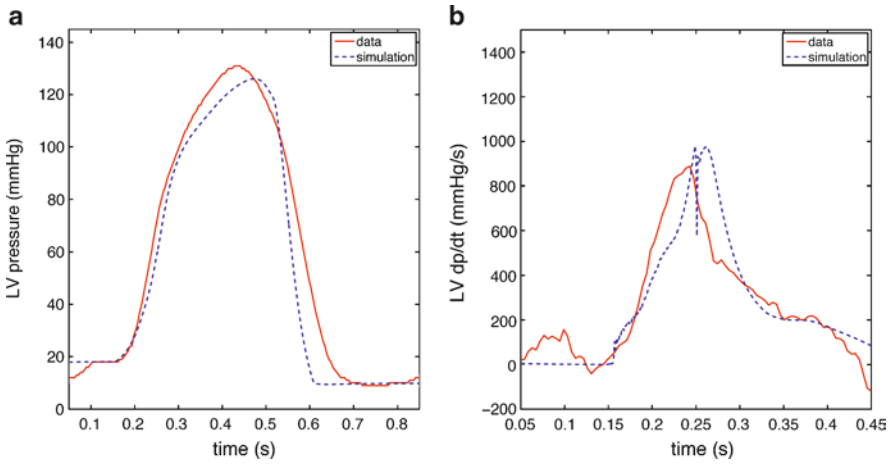

Fig. 10.7 (**a**) Measured (*solid*) and simulated (*dashed*) pressure curves in sinus rhythm. (**b**) Measured (*solid*) and simulated (*dashed*) d*P*/d*t* curves during systole in sinus rhythm

contractility parameters were decreased in the scar tissue. We then obtained a simulated motion relatively close to the one from the personalized kinematics. While there are still discrepancies, the general behavior is very similar. However, the automatic adjustment of local parameters is needed in order to be able to improve the fitting. The work in progress on this automatic identification is very promising [35, 53].

This personalized mechanical model produces simulated pressure in very good agreement with the catheter measurement (Fig. 10.7).

10.6 Prediction of the Acute Effects of Pacing on Left Ventricular Pressure

During the electrophysiology study, different pacing conditions are tested to evaluate the effect of different pacing lead locations and delays. This also gives the opportunity to estimate what could be the expected benefit from the pacemaker implantation. There is still a lot of research on what is the optimal number of electrodes, where are the optimal locations, and what are the optimal delays. This creates a large number of degrees of freedom that are difficult to optimize during the intervention itself. Being able to perform this optimization a priori and using an in silico model would be very useful.

In this section, we test the ability of our personalized electromechanical model of the myocardium to predict the changes in the heart due to a new pacing condition. The pacing protocol tested is biventricular pacing with simultaneous endocardial left ventricular pacing (we will call here this pacing sequence P1TRIV).

For the mechanical simulation, we use here the model personalized in Sect. 10.5.2 on baseline in sinus rhythm without changing any parameter. We then input the new

Table 10.1 Measured and simulated values for (dP/dt_{max}) in mmHg/s for five different conditions

	Sinus rhythm	Atrial	Right ventricle	LV endocardium	P1TRIV
Measurement	890	960	1,020	1,410	1,450
Simulation	910	970	1,000	1,480	1,440

electrical command corresponding to the pacing. The volumetric isochrones were derived as described in Sect. 10.4. We then observe the resulting simulated pressure curve allowing to test in particular predictions on the slope of this pressure during isovolumetric contraction. As this is the major cardiac phase that is sought to be optimized by CRT, we mainly focus on the model predictive power during this phase, and early ejection.

When simulating this P1TRIV pacing with the model personalized from baseline measurements, we observe a very good agreement of the pressure curve with the recorded data from the pressure catheter, and the dP/dt curve is also very similar. From the data, we can see that dP/dt_{max} goes from 890 mmHg/s at baseline to 1,450 mmHg/s for P1TRIV pacing. In the simulations we obtain 910 mmHg/s at baseline and 1,440 mmHg/s with pacing. So we can see that the improvement of the cardiac function brought by the pacing is well predicted by the in silico simulations. We used this methodology on four different pacing modes, with very promising results on the model predictions (Table 10.1).

10.7 Conclusion

We presented the personalization of a complete electromechanical model of the myocardium using XMR interventional data and how this personalized model could be used to predict therapy effects. The behavior of the model in sinus rhythm as well as the predictions of the model under pacing compare well with the measured data, which make such an approach very promising. This is the first case study demonstrating how models of the heart can be adjusted to be patient-specific and a first proof of concept of how this approach can be useful for therapy planning. While several steps still require interactive adjustment, the methodology for automatic parameter estimation is becoming available [8, 35, 53]. By integrating information about the anatomy, the electrophysiology, the kinematics, and the mechanics, we can explore the correlation between these different aspects for a given patient in order to provide an integrated view of the patient cardiac function and simulate and evaluate different therapies before their actual application. In the case of CRT, such predictions could help optimize in silico the pacemaker settings, which include the pacing lead locations and the delays between the electrodes. This will be the purpose of a future work.

Acknowledgments The authors would like to thank their co-workers in this project: R. Chabiniok, P. Chinchapatnam, T. Mansi, F. Billet, P. Moireau, J.M. Peyrat, K. Rhode, M. Ginks, P. Lambiase, S. Arridge, H. Delingette, M. Sorine, C.A. Rinaldi, D. Chapelle, and N. Ayache.

References

1. Aliev, R., Panfilov, A.: A simple two-variable model of cardiac excitation. Chaos, Solitons and Fractals 7(3), 293–301 (1996).
2. Beeler, G.W., Reuter, H.: Reconstruction of the action potential of ventricular myocardial fibers. Journal of Physiology 268, 177–210 (1977).
3. Beshai, J.F., Grimm, R.A., Nagueh, S.F., Baker, J.H., Beau, S.L., Greenberg, S.M., Pires, L.A., Tchou, P.J.: Cardiac-resynchronization therapy in heart failure with narrow QRS complexes. The New England Journal of Medicine 357(24), 2461–2471 (2007).
4. Bestel, J., Clément, F., Sorine, M.: A biomechanical model of muscle contraction. In: W. Niessen, M. Viergever (eds.) Medical Image Computing and Computer-Assisted intervention (MICCAI'01), *Lecture Notes in Computer Science (LNCS)*, vol. 2208, pp. 1159–1161. Springer-Verlag, Berlin, Germany (2001).
5. Billet, F., Sermesant, M., Delingette, H., Ayache, N.: Cardiac Motion Recovery and Boundary Conditions Estimation by Coupling an Electromechanical Model and Cine-MRI Data. In: Proceedings of Functional Imaging and Modeling of the Heart 2009 (FIMH'09), Lecture Notes in Computer Science (LNCS), vol. 5528, pp. 376–385, Nice, France, 3–5 June 2009.
6. Caillerie, D., Mourad, A., Raoult, A.: Cell-to-muscle homogenization. Application to a constitutive law for the myocardium. Mathematical Modeling and Numerical Analysis 37(4), 681–698 (2003).
7. Chapelle, D., Clément, F., Génot, F., Tallec, P.L., Sorine, M., Urquiza, J.: A physiologically-based model for the active cardiac muscle contraction. In: T. Katila, I. Magnin, P. Clarysse, J. Montagnat, J. Nenonen (eds.) Functional Imaging and Modeling of the Heart (FIMH'01), no. 2230 in *Lecture Notes in Computer Science (LNCS)*, pp. 128–133. Springer, Berlin (2001).
8. Chinchapatnam, P., Rhode, K., Ginks, M., Rinaldi, C., Lambiase, P., Razavi, R., Arridge, S., Sermesant, M.: Model-based imaging of cardiac apparent conductivity and local conduction velocity for diagnosis and planning of therapy. IEEE Transactions on Medical Imaging 27(11), 1631–1642 (2008).
9. Chinchapatnam, P.P., Rhode, K.S., King, A., Gao, G., Ma, Y., Schaeffter, T., Hawkes, D., Razavi, R.S., Hill, D.L., Arridge, S., Sermesant, M.: Anisotropic wave propagation and apparent conductivity estimation in a fast electrophysiological model: application to XMR interventional imaging. Medical Image Computing and Computer-Assisted Intervention: International Conference on Medical Image Computing and Computer-Assisted Intervention, 10, 575–583 (2007).
10. Chung, E.S., Leon, A.R., Tavazzi, L., Sun, J.P., Nihoyannopoulos, P., Merlino, J., Abraham, W.T., Ghio, S., Leclercq, C., Bax, J.J., Yu, C.M., Gorcsan, J., St John Sutton, M., De Sutter, J., Murillo, J.: Results of the predictors of response to crt (PROSPECT) trial. Circulation 117(20), 2608–2616 (2008).
11. Colli Franzone, P., Guerri, L., Rovida, S.: Wavefront propagation in activation model of the anisotropic cardiac tissue: Asymptotic analysis and numerical simulations. Journal of Mathematical Biology 28(2), 121–176 (1990).
12. Crampin, E.J., Halstead, M., Hunter, P., Nielsen, P., Noble, D., Smith, N., Tawhai, M.: Computational physiology and the physiome project. Experimental Physiology 89(1), 1–26 (2004).
13. Dou, J., Reese, T.G., Tseng, W.Y.I., Wedeen, V.J.: Cardiac Diffusion MRI without motion effects. Magnetic Resonance in Medicine 48(1), 105–114 (2002).
14. Ecabert, O., Peters, J., Schramm, H., Lorenz, C., von Berg, J., Walker, M.J., Vembar, M., Olszewski, M.E., Subramanyan, K., Lavi, G., Weese, J.: Automatic model-based segmentation of the heart in ct images. IEEE Transactions on Medical Imaging 27(9), 1189–1201 (2008).

15. Faris, O., Evans, F., Ennis, D., Helm, P., Taylor, J., Chesnick, A., Guttman, M., Ozturk, C., McVeigh, E.: Novel technique for cardiac electromechanical mapping with magnetic resonance imaging tagging and an epicardial electrode sock. Annals of Biomedical Engineering 31(4), 430–440 (2003).
16. FitzHugh, R.: Impulses and physiological states in theoretical models of nerve membrane. Biophysical Journal 1, 445–466 (1961).
17. Hill, A.: The heat of shortening and the dynamic constants in muscle. Proceedings of the Royal Society of London, Series B 126, 136–195 (1938).
18. Hodgkin, A., Huxley, A.: A quantitative description of membrane current and its application to conduction and excitation in nerve. Journal of Physiology 177, 500–544 (1952).
19. Humphrey, J.: Cardiovascular Solid Mechanics. Springer, Berlin (2002).
20. Humphrey, J., Strumpf, R., Yin, F.: Determination of a constitutive relation for passive myocardium: I. A new functional form. ASME Journal of Biomechanical Engineering 112, 333–339 (1990).
21. Hunter, P., McCulloch, A., Keurs, H.: Modeling the mechanical properties of cardiac muscle. Progress in Biophysics and Molecular Biology 69, 289–331 (1998).
22. Hunter, P., Nash, M., Sands, G.: Computational Biology of the Heart, chap. 12: Computational Electromechanics of the Heart, pp. 345–407. John Wiley & Sons Ltd, West Sussex, UK (1997).
23. Hunter, P., Nielsen, P.: A strategy for integrative computational physiology. Physiology (Bethesda) 20, 316–325 (2005).
24. Hunter, P., Pullan, A., Smaill, B.: Modeling total heart function. Annual Review of Biomedical Engineering 5, 147–177 (2003).
25. Keener, J., Sneyd, J.: Mathematical Physiology. Springer, Berlin (1998).
26. Kerckhoffs, R.C., Lumens, J., Vernooy, K., Omens, J.H., Mulligan, L.J., Delhaas, T., Arts, T., McCulloch, A.D., Prinzen, F.W.: Cardiac resynchronization: Insight from experimental and computational models. Progress in Biophysics and Molecular Biology 97(2–3), 543–561 (2008).
27. Kerckhoffs, R.C., McCulloch, A.D., Omens, J.H., Mulligan, L.J.: Effects of biventricular pacing and scar size in a computational model of the failing heart with left bundle branch block. Medical Image Analysis 13(2), 362–369 (2009).
28. Kilner, P., Yang, G., Wilkes, A., Mohiaddin, R., Firmin, D., Yacoub, M.: Asymmetric redirection of flow through the heart. Nature 404, 759–761 (2000).
29. Le Tallec, P.: Numerical methods for nonlinear three-dimensional elasticity. In: P. Ciarlet, J.L. Lions (eds.) Handbook of Numerical Analysis, vol. 3. Elsevier, North-Holland (1994).
30. Luo, C., Rudy, Y.: A model of the ventricular cardiac action potential: depolarization, repolarization, and their interaction. Circulation Research 68, 1501–1526 (1991).
31. MacLeod, R., Yilmaz, B., Taccardi, B., Punske, B., Serinagaolu, Y., Brooks, D.: Direct and inverse methods for cardiac mapping using multielectrode catheter measurements. Journal of Biomedizinische Technik 46, 207–209 (2001).
32. Masood, S., Yang, G., Pennell, D., Firmin, D.: Investigating intrinsic myocardial mechanics: the role of MR tagging, velocity phase mapping and diffusion imaging. Journal of Magnetic Resonance Imaging 12(6), 873–883 (2000).
33. McCulloch, A., Bassingthwaighte, J., Hunter, P., Noble, D., Blundell, T., Pawson, T.: Computational biology of the heart: From structure to function. Progress in Biophysics and Molecular Biology 69(2/3), 151–559 (1998).
34. McInerney, T., Terzopoulos, D.: Deformable models in medical images analysis: a survey. Medical Image Analysis 1(2), 91–108 (1996).
35. Moireau, P., Chapelle, D., Le Tallec, P.: Joint state and parameter estimation for distributed mechanical systems. Computer Methods in Applied Mechanics and Engineering 197, 659–677 (2008).
36. Montagnat, J., Delingette, H.: 4D deformable models with temporal constraints: application to 4D cardiac image segmentation. Medical Image Analysis 9(1), 87–100 (2005).

37. Moreau-Villéger, V., Delingette, H., Sermesant, M., Ashikaga, H., McVeigh, E., Ayache, N.: Building maps of local apparent conductivity of the epicardium with a 2D electrophysiological model of the heart. IEEE Transactions on Biomedical Engineering 53(8), 1457–1466 (2006).
38. Nash, M.: Mechanics and material properties of the heart using an anatomically accurate mathematical model. Ph.D. thesis, University of Auckland (1998).
39. Nickerson, D., Nash, M., Nielsen, P., Smith, N., Hunter, P.: Computational multiscale modeling in the IUPS physiome project: modeling cardiac electromechanics. Systems Biology 50(6), 617–630 (2006).
40. Nielsen, P., Grice, I.L., Smail, B., Hunter, P.: Mathematical Model of Geometry and Fibrous Structure of the Heart. American Journal of Physiology -Heart and Circulatory Physiology 260(29), H1365–H1378 (1991).
41. Noble, D.: A modification of the Hodgkin–Huxley equations applicable to purkinje fiber action and pace-maker potentials. Journal of Physiology 160, 317–352 (1962).
42. Noble, D.: Modeling the heart. Physiology 19, 191–197 (2004).
43. Noble, D., Varghese, A., Kohl, P., Noble, P.: Improved guinea-pig ventricular cell model incorporating a diadic space, *IKr* and *IKs*, and length and tension dependent processes. Canadian Journal of Cardiology 14, 123–134 (1998).
44. Park, J., Metaxas, D., Axel, L.: Analysis of left ventricular wall motion based on volumetric deformable models and MRI-SPAMM. Medical Image Analysis 1, 53–71 (1996).
45. Peyrat, J.M., Sermesant, M., Pennec, X., Delingette, H., Xu, C., McVeigh, E.R., Ayache, N.: A computational framework for the statistical analysis of cardiac diffusion tensors: Application to a small database of canine hearts. IEEE Transactions on Medical Imaging 26(11), 1500–1514 (2007). doi: 10.1109/TMI.2007.907286.
46. Peyrat, J.M., Sermesant, M., Pennec, X., Delingette, H., Xu, C., McVeigh, E.R., Ayache, N.: Statistical Comparison of Cardiac Fiber Architectures. In: Proceedings of the 4th International Conference on Functional Imaging and Modeling of the Heart (FIMH'07), vol. 4466 of LNCS, pp. 413–423 (2007).
47. Pollard, A., Hooke, N., Henriquez, C.: Cardiac propagation simulation. Critical Reviews in Biomedical Engineering 20(3,4), 171–210 (1992).
48. Rhode, K., Sermesant, M., Brogan, D., Hegde, S., Hipwell, J., Lambiase, P., Rosenthal, E., Bucknall, C., Qureshi, S., Gill, J., Razavi, R., Hill, D.: A system for real-time XMR guided cardiovascular intervention. IEEE Transactions on Medical Imaging 24(11), 1428–1440 (2005).
49. Sachse, F.B.: Computational Cardiology, Modeling of Anatomy, Electrophysiology, and Mechanics, *Lecture Notes in Computer Science*, vol. 2966. Springer, Berlin (2004).
50. Sainte-Marie, J., Chapelle, D., Cimrman, R., Sorine, M.: Modeling and estimation of the cardiac electromechanical activity. Computers and Structures 84, 1743–1759 (2006).
51. Sermesant, M., Delingette, H., Ayache, N.: An electromechanical model of the heart for image analysis and simulation. IEEE Transactions in Medical Imaging 25(5), 612–625 (2006).
52. Sermesant, M., Konukoglu, E., Delingette, H., Coudiere, Y., Chinchaptanam, P., Rhode, K., Razavi, R., Ayache, N.: An anisotropic multi-front fast marching method for real-time simulation of cardiac electrophysiology. In: Proceedings of Functional Imaging and Modeling of the Heart 2007 (FIMH'07), *LNCS*, vol. 4466, pp. 160–169 (2007).
53. Sermesant, M., Moireau, P., Camara, O., Sainte-Marie, J., Andriantsimiavona, R., Cimrman, R., Hill, D.L., Chapelle, D., Razavi, R.: Cardiac function estimation from MRI using a heart model and data assimilation: advances and difficulties. Medical Image Analysis 10(4), 642–656 (2006).
54. Sermesant M, Billet F, Chabiniok R, Mansi T, Chinchapatnam P, Moireau P, Peyrat JM, Rhode K, Ginks M, Lambiase P, Arridge S, Delingette H, Sorine M, Rinaldi A, Chapelle D, Razavi R, Ayache N. Personalised Electromechanical Model of the Heart for the Prediction of the Acute Effects of Cardiac Resynchronisation Therapy. In: Proceedings of Functional Imaging and Modeling of the Heart 2009 (FIMH'09), *LCNS,* vol. 5528, pp. 239–248 (2009).
55. Smith, N., Nickerson, D., Crampin, E., Hunter, P.: Computational mechanics of the heart from tissue structure to ventricular function. Journal of Elasticity 61(1), 113–141 (2000).

56. Stergiopulos, N., Westerhof, B., Westerhof, N.: Total arterial inertance as the fourth element of the windkessel model. American Journal of Physiology 276, H81–H88 (1999).
57. Streeter, D.: Gross Morphology and Fiber Geometry of the Heart. In: R. Berne (ed.) Handbook of Physiology, chap. The Cardiovascular System, Williams & Wilkins, Baltimore (1979).
58. Sutton, M.S., Keane, M.G.: Reverse remodeling in heart failure with cardiac resynchronization therapy. Heart 93(2), 167–171 (2007). doi: 10.1136/hrt.2005.067967.
59. Ten Tusscher, K., Noble, D., Noble, P., Panfilov, A.: A model of the human ventricular myocyte. American Journal of Physiology -Heart and Circulatory Physiology 286(4), 1573–1589 (2004).
60. Tomlinson, K.: Finite element solution of an eikonal equation for excitation wavefront propagation in ventricular myocardium. Ph.D. thesis, University of Auckland (2000).
61. Toussaint, N., Mansi, T., Delingette, H., Ayache, N., Sermesant, M.: An Integrated Platform for Dynamic Cardiac Simulation and Image Processing: Application to Personalized Tetralogy of Fallot Simulation. In: Proceedings of the Eurographics Workshop on Visual Computing for Biomedicine (VCBM). Delft, The Netherlands (2008).
62. Turk, G., O'Brien, J.: Variational implicit surfaces. Tech. rep., Georgia Institute of Technology (1999).
63. Xia, L., Huo, M.: Analysis of ventricular wall motion based on an electromechanical biventricular model. In: A. Murray (ed.) Computers in Cardiology, pp. 315–318. IEEE, New York NY, USA (2003).